Arousal neurons that anticipate deviations in blood glucose

Paulius Viskaitis[1], Alexander L. Tesmer[1], Mahesh M. Karnani[2], Myrtha Arnold[1], Dane Donegan[1], Ed F. Bracey[1], Daria Peleg-Raibstein[1], and Denis Burdakov[1]

[1]Institute for Neuroscience, Department of Health Sciences and Technology, ETH Zurich, Switzerland
[2]Faculty of Science, Integrative Neurophysiology, Vrije Universiteit Amsterdam, Netherlands

Abstract

The brain needs to track body energy state to optimize physiology and behavior. Important information about current and future energy states is contained in minute-to-minute fluctuations in blood glucose. However, it is unclear whether brain glucose sensors are capable of responding to this temporal structure to extract such information. In behaving mammals, hypothalamic hypocretin/orexin neurons (HONs) control arousal and are proposed to sense energy balance, yet recent studies show that HON activity varies rapidly (over seconds) with locomotion. It remains unknown if and how HONs reflect blood glucose fluctuations. Here, for the first time, we co-monitored HON activity and blood glucose in behaving mice, uncovering inhibition of HONs by rising blood glucose. Surprisingly, peak HON signals (population waves) anticipated peak glucose deviations by several minutes. In multivariate analysis of diverse HON activity correlates (locomotion, metabolic variables), the glucose temporal gradient (negative first derivative) emerged as prime predictor of HON population activity on the minute timescales, thereby explaining this anticipatory response. Furthermore, 2-photon imaging of >900 individual HONs revealed parallel communication of absolute blood glucose values and their derivatives in distinct HON subsets. Thus, HONs transmit multiplexed slowly and rapidly changing information, and, in the slow bandwidth, extract temporal features from blood glucose dynamics that suggest a hybrid of anticipatory and proportional logic in brain responses to blood glucose.

Orexin | Hypocretin | Lateral hypothalamus | Glucose
Correspondence: ***denis.burdakov@hest.ethz.ch***

Introduction

Blood glucose is a fundamental vital variable in our bodies. It is released into the blood and taken up by tissues, resulting in fluctuations in circulating glucose levels on the time scale of minutes. These fluctuations predict and determine healthy and maladaptive physiological states (1–4). How to measure and interpret blood glucose variability has thus been a key focus of research in biology, medicine, and engineering (5–8). Knowing current glucose provides feedback information about available energy, however, for timely responses, it is also vitally important to predict future states. Future states can be inferred from the rate of change of a parameter (9). Therefore, the temporal derivative of blood glucose carries valuable information about future glycemic state (7, 10). Indeed, reactive (feedback) and predictive (feedforward) control based on current states and derivatives of glucose improves performance of medical devices, such as the artificial pancreas (9–11). This raises an unanswered question: which features of blood glucose variability are sensed by the body's own glucose-measuring systems, such as the brain's glucose-sensing neurons (12–14)?

Here, we address this question at the level of a genetically-defined group of putative glucose-sensing neurons - the hypothalamic orexin/hypocretin neurons (HONs). These brain-wide projecting neurons promote wakefulness and orchestrate adaptive physiology across species (15). Their loss produces an inability to adapt arousal to body energy balance, as well as narcoleptic wakefulness instability and energy disorders (16–19). Studies of isolated HONs *in vitro* have shown that their activity is inhibited by step-like elevations in ambient glucose through mechanisms distinct from the use of glucose as an energy source (17, 20, 21). However, *in vivo*, such step-like changes in glucose level do not occur in the blood, and HONs receive multiple neural inputs, creating rapid HON modulation corresponding to locomotion and diverse sensory cues (17, 20, 22–24). Furthermore, HONs are also implicated in temperature regulation and respiratory control (25, 26). It is unknown whether and how HONs multiplex such diverse variables *in vivo*, and what features (if any) of blood glucose HONs sense in intact organisms.

Since blood glucose is rapidly regulated in intact organisms, changes in blood glucose levels cannot be inferred from an administered amount of glucose. Addressing this knowledge gap requires concurrent measurements of blood glucose and HON activity in behaving animals, at sufficient temporal resolution to capture their physiological dynamics. Here, for the first time, we perform such measurements, and visualize blood glucose responses of the HON population, as well as of >900 individual HONs.

Results

Blood glucose controls HONs and HON-dependent behavior *in vivo*. To track HON population activity in behaving mice, we used fiber photometry of GCaMP6s neural activity indicator selectively targeted to the HONs. We combined this with simultaneous telemetry, calorimetry, and locomotion recordings (Figure 1A, B; see Methods). We thus achieved multivariate, time-resolved phenotyping comprising orexin-GCaMP6s signal, blood glucose, body temperature, respiratory exchange ratio, energy expenditure, and locomotion (Figure 1C).

We then analyzed the responses of these variables to blood glucose fluctuations (see Methods). We initially quantified these responses by comparing how glucose vs saline infusions affected the mean value of each sampled variable during 5-25 minutes post-infusion (Figure 1D-I). This revealed that HONs were inhibited (Figure 1D) by glucose infusions that elevated blood glucose (Figure 1E), body temperature (Figure 1F), and respiratory exchange ratio (Figure 1G).
Consistent with reports that HON activation stimulates locomotion (27), we found that glucose-induced HON inhibition was associated with a reduction in locomotion (Figure 1I). To test whether the glucose-induced reduction of locomotion required HONs, we carried out experiments in HON-ablated mice (see Methods), and found that in these mice glucose infusions failed to reduce locomotion (Supplementary Figure 1).
Together, these results demonstrate that blood glucose controls HONs *in vivo*, and confirm that HONs are important for appropriate behavioral responses to changes in blood glucose.

HON population activity represents a temporal derivative of blood glucose. We next examined temporal alignment of changes in HON activity and blood glucose. The prevailing hypothesis based on *in vitro* recordings of HON activity is that they are inhibited in proportion to ambient glucose concentration with a delay of several minutes (20). If this were true in the living organism, then – hypothetically – HON activity would be predicted to be a "temporal mirror image" of glucose with maximal HON inhibition occurring after glucose peak (Figure 2A, B), and a negative monotonic relation between HON activity and increasing glucose concentration (Figure 2C, Supplementary Figure 2).
However, our *in vivo* measurements did not conform to these predictions. HON population activity did not follow the glucose waveform, but instead fell only when glucose was rising, with peak HON response preceding peak glucose rise by several minutes (Figure 2D, E). HON activity subsequently returned to control (saline) level when glucose was highest and stable, and then rose when glucose was falling (Figure 1D, E; Figure 2D-F). From this unexpected temporal profile of HON glucose responses, we hypothesized that HON activity was negatively related to the glucose first derivative. Indeed, we found that the relationship between the glucose derivative and HON activity (Figure 2G-I) matched the hypothetical "delayed mirror" response (Figure 2A-C).
Overall, these data indicate that, at the population level, HON activity more closely reflects the rate of change, rather than absolute values of blood glucose levels.

Coding of motor, respiratory, and glucose variables in slow dynamics of HON population. After glucose infusions, mice displayed multiple physiological and behavioral responses (Figure 1). This, for the first time, gave us access to many physiological variables that are thought to be relevant to HONs, within the same behavioral paradigm. This enabled us to compare the relative influence of these variables on HON activity. To do this, we require a method to quantify how much variability of the cell responses can be attributed to each separate variable, despite the presence of multiple variables.
Towards this end, we quantitatively predicted the slow HON population activity based on the other physiological variables ("predictors") with an encoding model (28)(Figure 3A). Predictors also included the first derivatives of variables (Figure 3A), because this temporal feature was implicated in HON responses to glucose (Figure 2). Using this encoding model, we calculated the relative contribution of each physiological variable to the slow HON population response, by quantifying how much of the explained variance decreased when that variable was removed from the model (Figure 3B). The highest relative contribution was attributed to the derivative of glucose (52±3.5% relative contribution to explained variance), followed by consumed oxygen volume, (VO2, 37±6.3%), and by derivative of produced carbon dioxide volume (VCO2, 31±4.8%) (Figure 3C).
Thus, when co-variation of HON activity across multiple physicochemical and behavioral factors is considered, the glucose derivative emerges as a strong determinant of information transmitted by the HON population.

Parallel transmission of distinct temporal features of glucose variability in HON subsets. Is blood glucose represented similarly in every HON, or do subsets of HONs transmit distinct temporal features of glucose variability? The photometry measurements of HON population activity performed in Figures 1-3 do not distinguish between these alternatives, since any activity variations across cells are invisible in the net activity. To systematically examine this question, we switched our HON activity recording mode to single-cell resolution, by using 2-photon volumetric imaging of HONs through hypothalamus-implanted gradient index (GRIN) lenses (27) (Figure 4A).
We recorded the activity of 92-180 HONs simultaneously in each of 7 mice (Figure 4B; n = 913 HONs from 7 mice). The summed response of single cells to glucose (Figure 4C, D; saline control is shown in Supplementary Figure 3) resembled HON activity in population imaging (Figure 1D), indicating that HON glucose-sensing was preserved in both recording modes.
To compare glucose responses between individual cells, we fitted each cell's activity profile to several templates representing distinct temporal features of glucose dynamics, and classified cells based on best goodness-of-fit (Figure 5A, see Methods). Based on this classification, the majority of HONs (98%; 895/913 cells) responded to glucose, with only 2% of cells not fitting any of the templates (Figure 5B, D). Glucose-responsive HONs represented either actual or inverted-sign values of glucose (24.1% and 32% of the 913 HONs respectively, Figure 5B, D), or glucose derivatives (inverted-sign derivative, 30.7% of cells; derivative, 11.3% of cells respectively, Figure 5B, D). The HON subsets were largely intermingled within the recording volume (Figure 5E). As expected from the relative amplitudes and directions of the single-cell responses (Figure 5B, C), and consistent with population responses, the sum of all analyzed cells reflected the

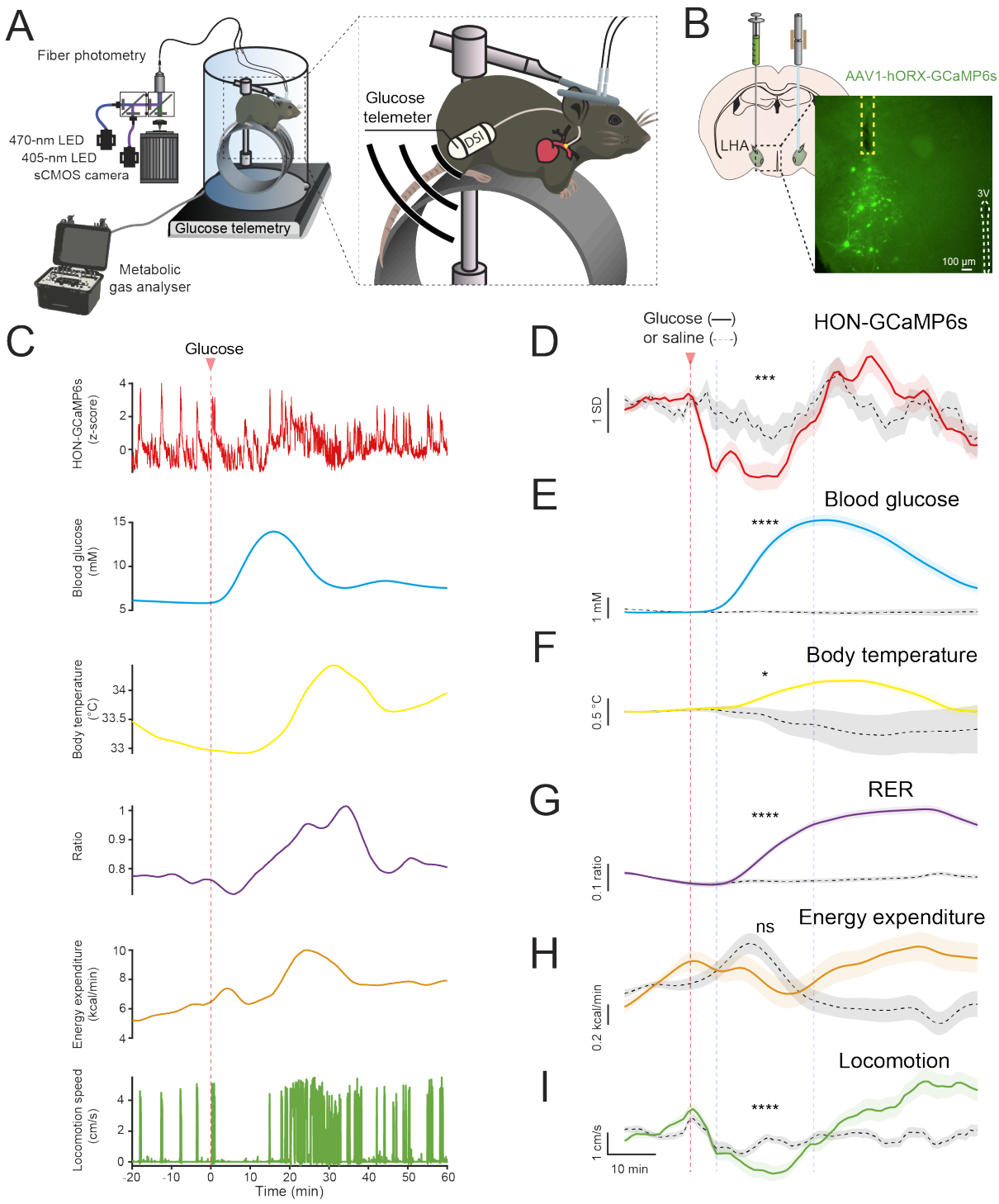

Figure 1. Simultaneous tracking of HON activity, metabolism, and locomotion.
(A) Schema of experimental setup for simultaneous fiber photometry, indirect calorimetry, glucose and temperature telemetry (DSI), and locomotion recordings. **(B)** Stereotaxic surgery schematic (left), LHA lateral hypothalamic area, and (right) expression of GCaMP6s in HONs for fiber photometry. The dashed square box indicates the fiber location. 3V, 3rd ventricle. **(C)** Example data from one recording session. **(D-I)** Group data for the experiment shown in C. Blue dotted lines indicate analysis period of 5 – 25 minutes from which mean values and statistics stated below are derived. Data smoothed by a 5-minute moving mean for visualization only. Compared to saline infusion, glucose injection: **D**, reduced HON activity responses (t-test $p < 0.001$; df = 69, tstat = 3.918; n = 39 & 32 responses from 13 and 10 animals to sal and glu respectively), **E**, increased blood glucose level (t-test $p < 0.0001$; df = 26, tstat = -5.563; n = 7 & 21 responses from 6 and 6 animals to sal and glu respectively), **F**, increased body temperature (t-test $p < 0.05$; df = 31, tstat = -2.598; n = 7 & 26 responses from 7 and 8 animals to sal and glu respectively), **G**, increased respiratory exchange ratio (RER) (t-test $p < 0.0001$; df = 87, tstat = -6.322; n = 59 & 30 responses from 30 and 15 animals to sal and glu respectively), **H**, did not alter energy expenditure (t-test $p = 0.08$; df = 87, tstat = 1.762; n = 59 & 30 responses from 30 and 15 animals to sal and glu respectively) and **I**, reduced running (t-test $p < 0.0001$; df = 117, tstat = 4.736; n = 80 & 39 responses from 32 and 19 animals to sal and glu respectively).
10-minute time bar shown in panel I applies to panels D-I. Data are presented as means and SEM; *$p < 0.05$, ***$p < 0.001$, and ****$p < 0.0001$; ns $p > 0.05$.

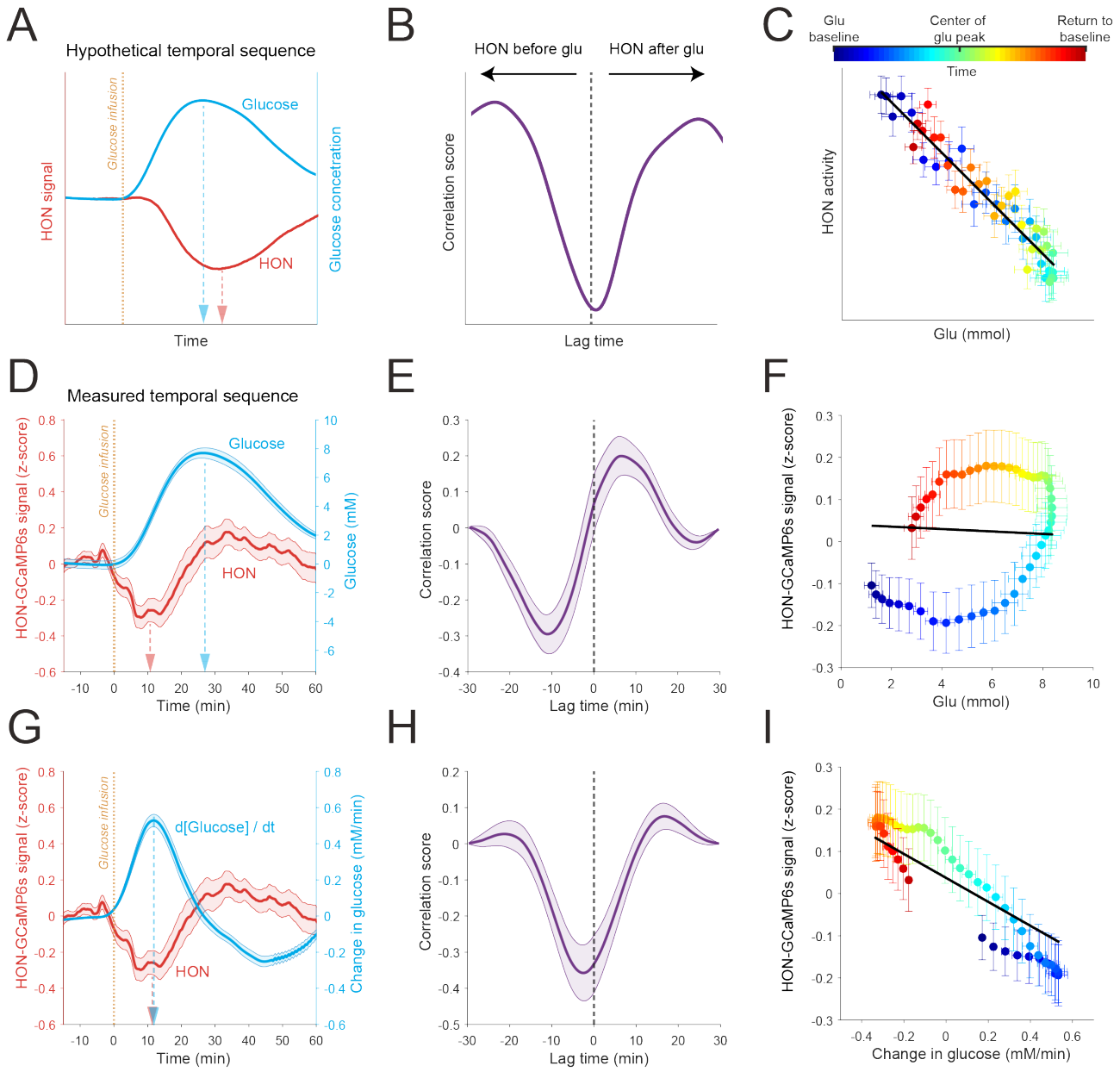

Figure 2. Temporal relations of HON population activity and blood glucose.
(A-C) Hypothetical temporal relations based on existing data (see Results text). **(D-F)** Measured temporal relations of HON activity and blood glucose, simultaneously recorded in the same experiments. (**D**) HON activity and blood glucose concentration traces; peak HON response preceded peak glucose concentration. (**E**) Cross-correlation. (**F**) Linear fit did not explain variability: R2 = 0, p = 0.288. **(G-I)** Measured temporal relations of HON activity and glucose derivative (d[Glucose]/dt]). Linear fit explained some variability and the slope was significantly non-zero (**I**): R2 = 0.04, p < 0.001.
In **D-I**, data are means and SEM of n = 139 intragastric glucose infusion responses from 22 mice. Data smoothed by a 10-minute moving mean for visualization.

inverted glucose derivative (Figure 4C).

Overall, this cellular-resolution analysis indicates that the HON population signal mirrors the inverted glucose derivative, while HON subsets extract multiple temporal features from blood glucose variability.

Discussion

The discovery of hypothalamic glucose-sensing neurons over half a century ago (29, 30) suggested a direct strategy for how the brain may sense body energy state. A central question in sensory systems is whether they simply relay their inputs, or extract specific temporal features from them (9, 31). For genetically-defined glucose-sensing neurons operating inside behaving organisms, this question also has not been answered.

Our data provide fundamental insights into how HONs react to real-time blood glucose variability. In behaving mice, HONs are not simply inhibited by blood glucose as previously assumed, but instead transmit multiple temporal features of blood glucose variability. At the population level, a dominant feature of glycemic variability encoded by HONs

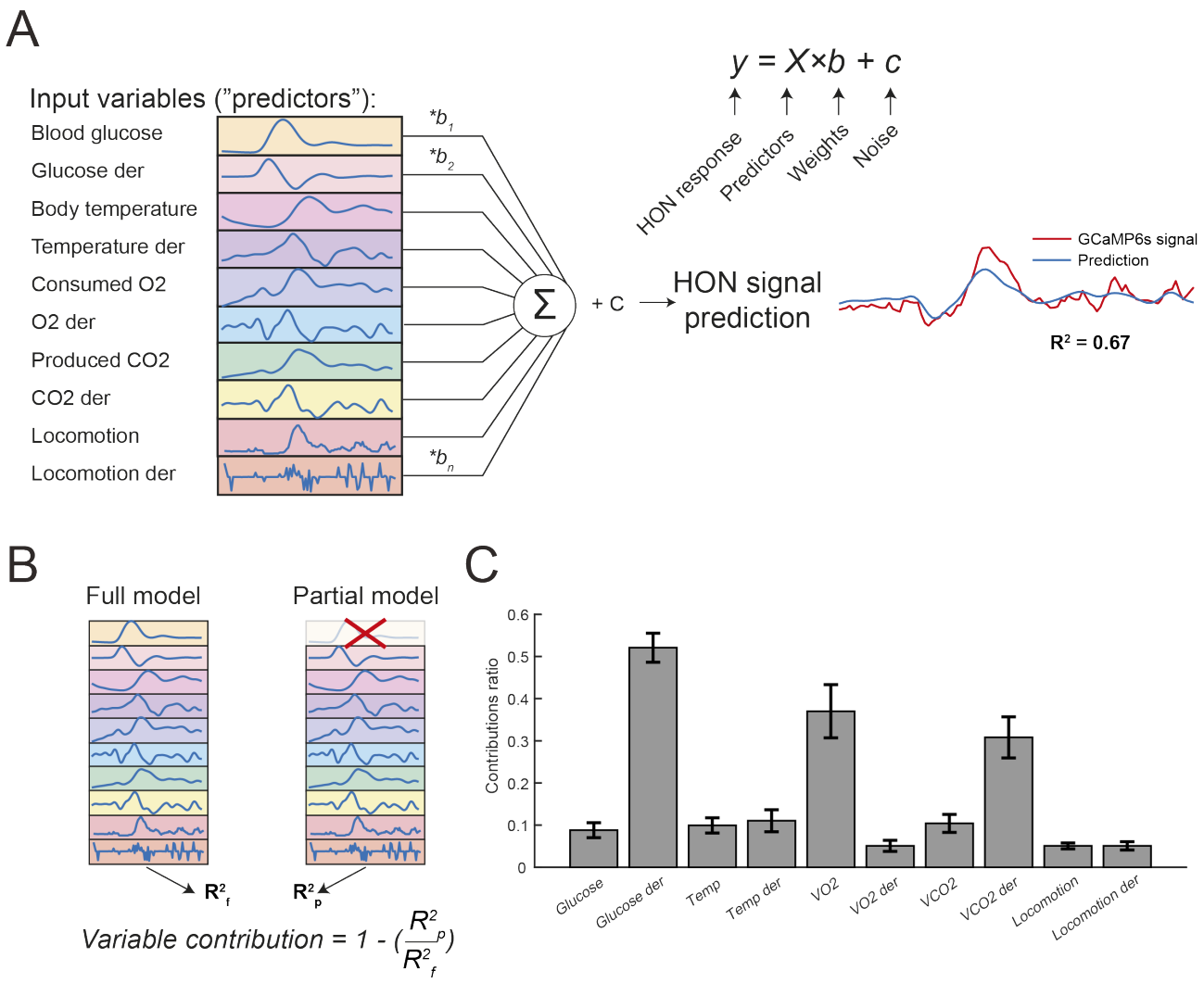

Figure 3. Quantifying HON responses to specific variables within multivariate experiments.
(A) Depiction of the general linear model workflow to predict HON activity from the simultaneously-measured (Figure 1) set of physiological variables. **(B)** Illustration of input variable contribution testing. **(C)** Ranking of input variable contributions for accuracy in modeling HON activity after glucose infusion.
Data are presented as means and SEM.

was its temporal gradient, specifically, the sign-inverted first derivative. This conclusion held even in the context of multivariate analysis of other factors proposed to be related to HON activity (locomotion, energy expenditure (27, 32)) (Figure 3). At the single-cell level, we discovered individual HONs that also relayed different temporal features of blood glucose variability, including signals reflecting glucose temporal derivatives, or absolute levels (Figure 5). To the best of our knowledge, such ability to send multiple streams of information about blood glucose within a genetically-defined cell population has not been previously reported.

What could be the evolutionary advantages of such HON responses to blood glucose? HONs are thought to engage the sympathetic system to convert body energy stores into blood glucose in association with behaviors such as locomotion which facilitates discovery of food sources; conversely, reduced HON activity promotes rest and energy storage (27, 33). Indeed, in mice without HONs, control of locomotion by blood glucose was disrupted (Figure S1). It is therefore possible that glucose-sensitive HONs are part of a controller that adjusts physiology to blood glucose. In engineering, proactive and reactive control signals – i.e. signals that vary in proportion to derivative and absolute values of a sensed input, respectively – achieve better control than simple reactive controllers (9). Because distinct HONs subsets relayed both proportional and derivative information about blood glucose (Figure 5), HONs might be a neural correlate of such a proportional-derivative controller. The derivative-based output may promote energy storage in proportion to how fast the glucose is rising, and may mobilize energy stores and exploratory behavior in proportion to how fast glucose is falling. The proportional output may reactively finetune physiological functions according to current glucose concentration.

These findings open interesting directions for further study. Downstream of HONs, it could be investigated whether HON

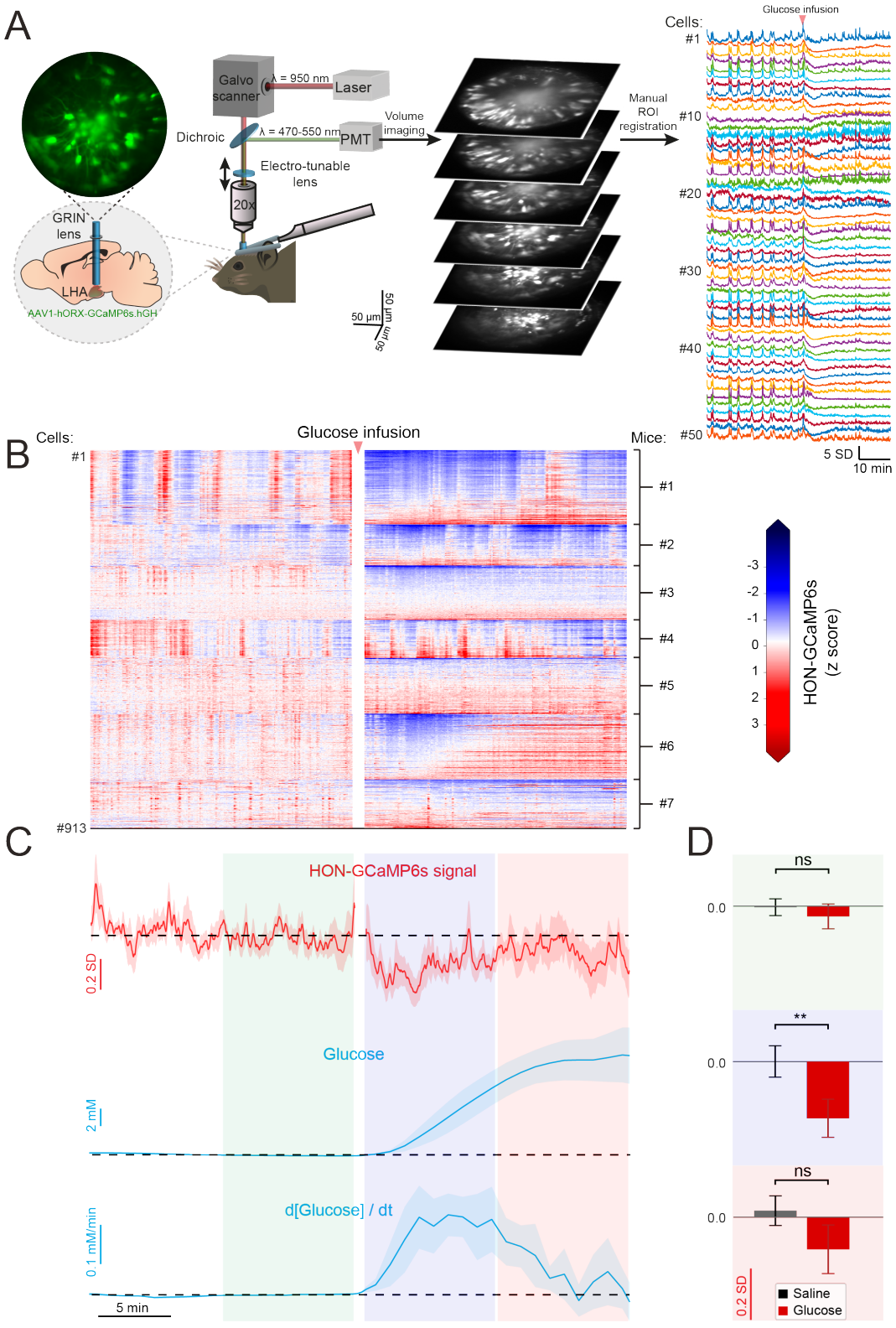

Figure 4. Visualizing responses of individual HONs to blood glucose fluctuations.

(A) Schema of 2-photon imaging of individual HONs in behaving mice. **(B)** Individual responses of 913 HONs to glucose infusion from 7 mice. **(C)** Temporal alignment of average HON responses (top) to blood glucose concentration (middle) and its derivative (bottom). **(D)** HONs are significantly inhibited only during high glucose derivative phase (between 2 and 11 minutes), but not during high absolute glucose (between 11 and 20 minutes) or during baseline periods (between -11 and -2 minutes). 2-way repeated measures ANOVA: treatment p = 0.029, F (1.0, 6.0) = 8.216; Šidák correction multiple comparisons: p = 0.709 (-11:-2), p = 0.005, (2:11), p = 0.534 (11:20); n = 7 mice.

Breaks in the neural activity recordings are due to laser shutter being closed during infusions in majority of the experiments. Data are presented as means and SEM; **p < 0.01 and ns p > 0.05.

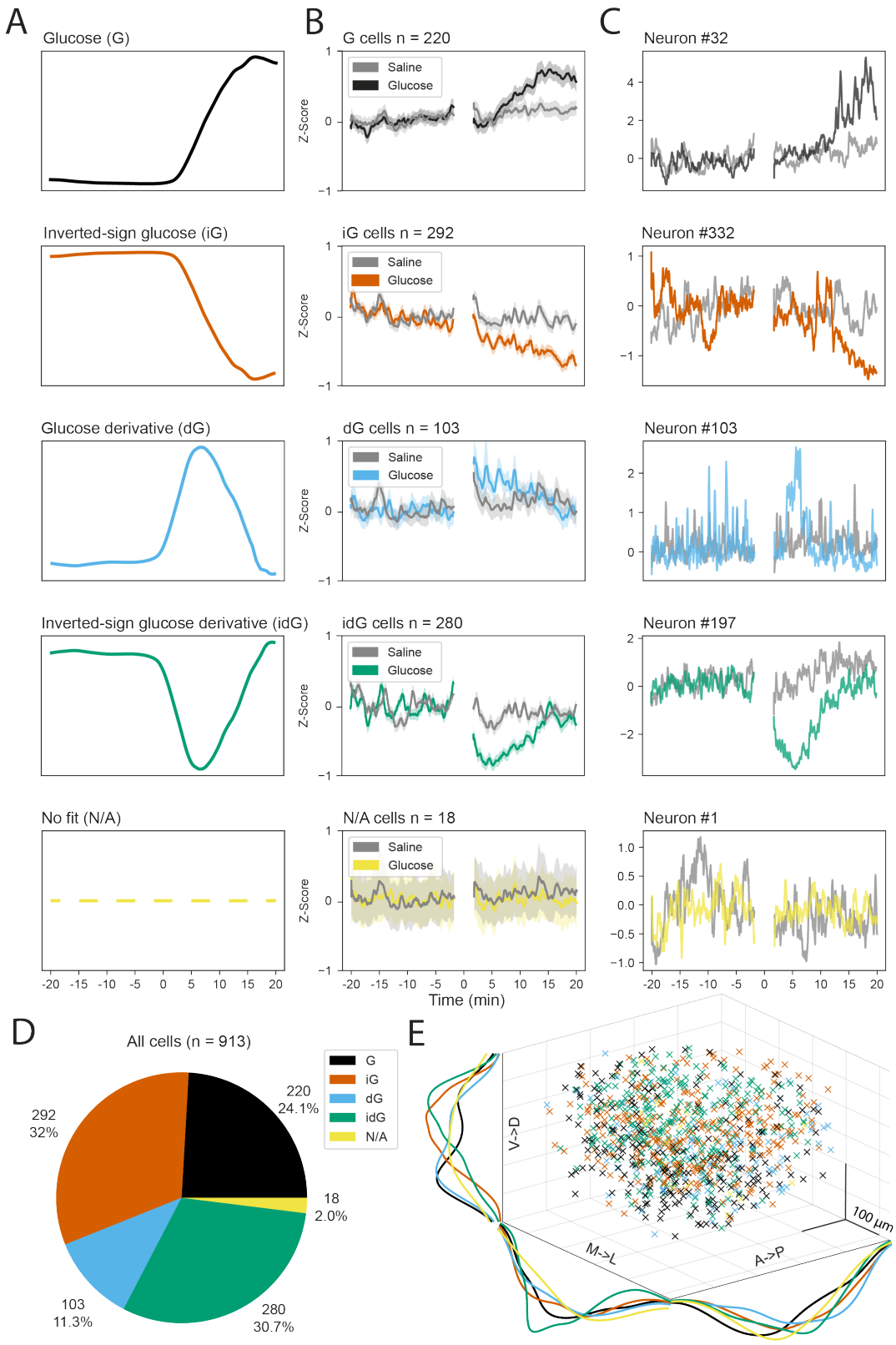

Figure 5. Classification of single-cell HON responses to blood glucose.
(A) Fitting templates based on recorded blood glucose dynamics: glucose (G), inverted glucose (iG), glucose derivative (dG), inverted glucose derivative (idG) and no fit (N/A, see Methods). **(B)** Average HON activity traces for each of the glucose-response classes. **(C)** Examples of individual neurons from each class. **(D)** Relative proportions of HON subsets. **(E)** Anatomical distribution of HON subsets.
Breaks in the neural recordings are due to laser shutter being closed during infusions in majority of the experiments. Data are presented as means and SEM.

subsets with distinct glucose responses engage distinct or overlapping decoders and effectors, e.g. glucose mobilization from the liver via the sympathetic system (34, 35), or control of movement and arousal (27, 36). Upstream of HONs, other glucose-interpreting systems presumably exist, since the *in vivo* diversity in HON glucose representations (Figure 5) is not apparent in HONs *in vitro* (17, 20). Thus, HON encoding of blood glucose may arise through a combination of direct and indirect sensing whose relative contributions remain to be determined. Deeper knowledge of how precisely-defined neural classes and connections turn blood glucose into adaptive responses will facilitate insights into restoring disrupted glucose handling in patients (37), and into blood glucose-associated behavioral changes in healthy individuals (37).

ACKNOWLEDGEMENTS
This work was funded by ETH Zürich, and The Francis Crick Institute which receives its core funding from Cancer Research UK (FC001055), the UK Medical Research Council (FC001055), and the Wellcome Trust (FC001055).

METHODS

Experimental subjects. Animal studies followed United Kingdom Home Office regulations or Swiss Federal Food Safety and Veterinary Office Welfare Ordinance (TSchV 455.1, approved by the Zurich Cantonal Veterinary Office). Adult C57BL6 male mice were studied, thus whether conclusions apply to female mice remains to be determined. For HON deletion experiments (Supplementary figure 1), we used orexin-DTR mice as previously described (38, 39). Animals were housed in reversed light-dark cycle (lights off at 7:00 a.m.), and all experiments were performed during the dark phase. Animals had ad libitum access to food (3430 Maintenance Standard diet, Kliba-Nafag) and water, unless stated otherwise. Known effect sizes and variation were used for power calculations and determination of required number of animals, where possible, to maximize chances of meaningful results without the unnecessary use of the experimental animals. Studies were repeated in at least 2 independent cohorts and used a semi-randomized crossover design.

Surgeries and viral vectors. HON activity measurement was achieved with GCaMP6s cysotolic calcium indicator delivered using orexin promoter-containing AAV (AAV1-hORX-GCaMP6s.hGH; 10^{13}-10^{14}GC/ml, Vigene Biosciences) which targets HONs with >96% specificity (38). For fiber photometry studies, the GCaMP6s AAV was stereotaxically injected into the LH bilaterally (anteroposterior [AP], -1.35; mediolateral [ML], ±0.90; dorsoventral [DV], -5.70, -5.40 & -5.10, 70 nl per site) and optic fiber cannulae (0.2 mm diameter, 0.39 numerical aperture (NA) fiber with 1.25 mm ceramic ferrule; Thorlabs) were implanted above the LH (AP, -1.35; ML, ±0.90; DV, -5.00). For 2-photon imaging, the same virus and coordinates were used, but surgery was performed only on the left hemisphere and a GRIN lens (0.39 NA, 7.3 mm long, 0.6 mm, Inscopix) was slowly (150 µl/min) implanted instead of the cannulae. Implants and a custom-made aluminum head plate were secured to the skull using three skull screws and dental cement (Kemdent and C&B-Metabond).
For intragastric infusion experiments, the surgery was adapted from rats as previously described (39). A custom-made catheter was implanted by guiding tubing subcutaneously through the dorsal to the ventral incision. A fixation mesh was then positioned subcutaneously at the level of the scapula blades and catheter exited on the animal's back. To prevent damage, a custom-made cover was fixed on the animals after every experiment. To prevent catheter blockage, saline (0.1 ml) was used to flush catheters daily for 5 days and every second day until the end of the study. Catheter functionality was confirmed by the presence of back-flow after saline infusion and terminally by dissection. In the event of catheter blockage, subjects were excluded from further experiments, but the data collected prior to blockage were included in the analyses.
Glucose and temperature telemeters were implanted following the manufacturer's instructions (DSI) - glucose sensor entered the systemic blood system via the left carotid artery with 1.5 mm of the sensor protruding into the aorta. All surgeries were performed under aseptic conditions and animals received isoflurane anesthesia, as well as operative and postoperative analgesia.

Fiber photometry. For fiber photometry experiments (Figures 1-3), we used a custom camera-based photometry system (built with assistance of Dr. Dale Elgar, INSS and based on (40)). Alternating illumination of two excitation LEDs (405 nm and 465 nm at 20 Hz each, average power = 100 µW at implant fiber tip) was used to record LH HON-GCaMP6s emission fluorescence bilaterally, in 1-3 animals simultaneously. Emission generated by the 405 nm LED was used as a control for movement artefacts, the effects of which were further minimized by recording in habituated, head-fixed animals (Figure 1A). GCaMP6s bleaching, fiber illumination or expression variability were accounted for by de-trending and normalizing each trace as follows: 1) local minima of each trace were found ("convhull" function in Matlab); 2) a least-squares triple exponential was fit through the convex hull; 3) each trace was detrended by subtracting and dividing by its minima-fit; 4) each trace was z-score normalized based on its 20 minute pre-infusion standard deviation (SD) and mean.

2-photon imaging. Volumetric 2-photon imaging via GRIN lenses was performed as previously described (27). Excitation of GCaMP6s was achieved with a femtosecond-pulsed mode-locked Ti:sapphire laser (Spectra-physics Mai Tai HP Deepsee 2) at 950 nm. The emission fluorescence was imaged using a resonant/galvanometer scan head two-photon microscope (INSS), equipped with a 20× (0.45 NA, Olympus) air-IR objective, a custom electro-tunable lens and a 510/80nm band-pass emission filter. A volume of 512×512 pixels x6 planes was recorded at 5.1 volumes/s using a custom Labview software. Resultant image stacks were processed in FIJI, Matlab, and Python softwares as follows: 1) the imaged volume was separated into separate planes (and lens-transition plane was discarded from further analysis); 2) 2x2 binning and TurboReg (precise, rigid) motion correction

were applied; 3) cell outlines were manually drawn and labelled as regions of interest (ROIs); 4) ROI maps were applied across sessions within the same animal and adjusted; 5) ROIs that corresponded to the same cell in a plane or across neighboring planes were identified (in at least 2 independent experimental sessions, >5% ROI overlap of 3 pixel expanded contours, > 90% cross-correlation coefficient and <2s lag) and joined in further analysis; 6) HON cell activity was aligned based on saline/glucose infusion timing and same condition recordings were averaged per each cell individually. 7) HONs were assigned to glucose-response classes by fitting their activity profile to transformations of glucose dynamics (inverted-sign derivative, derivative, proportional, and inversely proportional); 8) classified cells were anatomically mapped.

For classification of HON activity to transformed glucose dynamics, templates were constructed using the average blood-glucose trace following IP-injection of 2 mg/kg glucose from mice not used in the classification. The mean trace was smoothed using a 1.5-minute window moving mean before relevant transformations were applied. If the transformation was a derivative, the template was smoothed again after differentiation using the same filter parameters. Cell activity traces were extracted and aligned to the first 20 minutes of the template-trace following IP injection. Only experiment-days with a 2mg/kg glucose injection were used for classification. By calculating the Pearson's Correlation Coefficient (PCC) of the extracted traces with each of these templates, we assigned cells to the response-class with the maximum PCC. A two-sided p-value was calculated alongside each correlation (SciPy library). Using the Bonferroni-adjustment for multiple comparisons, we classified responses that had no p-value with any template less than alpha = 0.001/4 as belonging to a fifth 'no fit' (N/A) category.

Concurrent monitoring of glucose, metabolic parameters, and locomotion. Blood glucose concentration and body temperature were measured with and pre-processed by HD-XG telemetry system (DSI). Metabolic measurements were obtained by recording continuous gas exchange in a custom enclosure by an adapted Field Metabolic System (Sable). Data was pre-processed in ExpeData software and exported for analysis in Matlab. Running of head-fixed animals was measured on a wheel using an optical encoder (Honeywell, 128 ppr 300rpm Axial). State changes of the encoder were recorded using a master Matlab code running photometry or Labview programs synced to the 2-photon microscope. All acquisition systems were synced via digital signals to the Matlab code running photometry or to the Labview 2-photon imaging program. All data was exported and further processed in Matlab. Simultaneous measurements were resampled to achieve the same acquisition rate of 1Hz. For visual clarity, Figure 1 data were smoothed with a 5 minute moving mean, and Figure 2 glucose and photometry data were smoothed with a 10 minute moving mean and down sampled to 20 seconds. To generate hysteresis plots, boundaries of the blood glucose peak were identified and 50 equally spaced points were taken (see Figure S2) to plot HON signal vs blood glucose level (Figure 2F) or vs blood glucose derivative (Figure 2I).

Input-output relations between neural activity and glucose. In our analyses of cell responses to glucose we used actual blood glucose values. In this way, we assessed the effects on neural activity of a large range of blood glucose concentrations (baseline range = 3.5-11.1 mM; baseline mean = 7.3±0.17 mM; glucose peak range = 11.1-34.9 mM, mean = 24±0.9 mM) and rates of change (range = 0.12-1.45 mM/min, mean of maximum rate of change = 0.56±0.03 mM/min). To achieve this range of glucose inputs and compare them to neural activity responses, the glucose infusions varied in both concentration and route of administration (intragastric or intraperitoneal). To improve accuracy and capture circulating glucose dynamics, we used direct measurements of blood glucose responses, rather than injected dosage values. For intragastric infusions, glucose infusion parameters were selected from a set of concentrations (0.08, 0.12, 0.146, 0.24 and 0.45 g/ml) and infusion speeds (50, 66.7, 90 and 180 µl/min) such that total infusion volume did not exceed 0.9 ml/ml or 0.45ml for fast infusions (180 µl/min). For intraperitoneal (IP) glucose infusions, 2 mg/kg dose at around 200 µl/min was achieved by varying infusion volume, generally between 100-150 µl. Combination of all infusion parameters were used to generate data analyzed in Figure 2, and the 0.24 mg/ml dose (delivered at 90 µl/min rate over 10 minutes) effects are demonstrated in Figures 1 and 3. 2mg/kg IP glucose was used in 2-photon analyses shown in Figures 4 and 5

Encoding model. To determine relative contributions of various behavioral and metabolic variables to HON responses, we used a generalized linear model approach, based on principles described before (28). For this model, HON population activity was used as the response variable, while predictor variables were running, blood glucose, body temperature, consumed O2 volume, produced CO2 volume and their derivatives with respect to time (Figure 3A). All variables were down-sampled to 1 minute in order to equalize their sampling rates and focus on the slow dynamics, Savitzky–Golay filtered (1st order, 5 sample window), and normalized by z-scoring. Resultant data was fit using "glmfit" function in Matlab by bootstrapping ¼ experiment-duration chunks randomly over 2000 iterations. Here 70% of data was used for training and 30% was used for validation on untrained data. Non-bootstrapping methods such as leave-one-out cross validation were also used to confirm the findings. For each fitting iteration, partial models based on the same training data but without a single independent variable were generated. Then a coefficient of determination (R2) was calculated for full and partial models on the validation data (either on the 30% of bootstrapped data or the left out experiment). We determined relative contribution of a given predictor to HON activity dynamics by comparing how much the encoding model performance has declined without a given variable - by comparing the R2 of the partial model to the R2 of the full model (Figure 3B). Negative relative contributions were set to zero, following the method described in (28).

Data analysis and statistics. Raw data was processed in Matlab. Statistical analysis was done in GraphPad Prism 9.0, Matlab or Python. Key comparisons between saline and glucose (Figures 1 and 4) and cell classification (Figure 5) were performed on raw, non-smoothed data. Sample size, statistical tests used and their results are indicated in the figures, their legends and/or their descriptions in the text. Statistical comparisons were performed on non-filtered data, but some traces were filtered for visual purposes, as indicated. Statistical analysis was based on settings recommended by GraphPad Prism 9.0. P values of <0.05 were considered significant. Where significance is presented, p values are as follows: *p<0.05, **p<0.01, ***p<0.001, and ****p<0.0001, ns = p>0.05. Outliers that failed a ROUT 1% test were removed. Data are presented as means and standard error of the mean (SEM) unless stated otherwise.

Bibliography

1. Matthew T. Gailliot and Roy F. Baumeister. The Physiology of Willpower: Linking Blood Glucose to Self-Control. *Personality and Social Psychology Review*, 11(4):303–327, nov 2007. ISSN 1088-8683. doi: 10.1177/1088868307303030.
2. Zheng Zhou, Bao Sun, Shiqiong Huang, Chunsheng Zhu, and Meng Bian. Glycemic variability: adverse clinical outcomes and how to improve it? *Cardiovascular Diabetology*, 19 (1):102, dec 2020. ISSN 1475-2840. doi: 10.1186/s12933-020-01085-6.
3. Claude Messier and Michèle Gagnon. Glucose regulation and cognitive functions: relation to Alzheimer's disease and diabetes. *Behavioural Brain Research*, 75(1-2):1–11, feb 1996. ISSN 01664328. doi: 10.1016/0166-4328(95)00153-0.
4. Paul E. Gold. Role of glucose in regulating the brain and cognition. *The American Journal of Clinical Nutrition*, 61(4):987S–995S, apr 1995. ISSN 0002-9165. doi: 10.1093/ajcn/61.4.987S.
5. Philipp Mergenthaler, Ute Lindauer, Gerald A. Dienel, and Andreas Meisel. Sugar for the brain: the role of glucose in physiological and pathological brain function. *Trends in Neurosciences*, 36(10):587–597, oct 2013. ISSN 01662236. doi: 10.1016/j.tins.2013.07.001.
6. David Rodbard. Glucose Variability: A Review of Clinical Applications and Research Developments. *Diabetes Technology Therapeutics*, 20(S2):S2–5–S2–15, jun 2018. ISSN 1520-9156. doi: 10.1089/dia.2018.0092.
7. Claudio Cobelli, Eric Renard, and Boris Kovatchev. Artificial Pancreas: Past, Present, Future. *Diabetes*, 60(11):2672–2682, nov 2011. ISSN 0012-1797. doi: 10.2337/db11-0654.
8. Arthur L. Campfield and Françoise J. Smith. Blood glucose dynamics and control of meal initiation: a pattern detection and recognition theory. *Physiological reviews*, 83(1):25–58, jan 2003. ISSN 0031-9333. doi: 10.1152/physrev.00019.2002.
9. Allen Stubberud, Ivan Williams, and Joseph DiStefano. *Schaum's Outline of Feedback and Control Systems*. McGraw-Hill, 2 edition, 2012. ISBN 9780070170520.
10. Gianni Marchetti, Massimiliano Barolo, Lois Jovanovic, Howard Zisser, and Dale E. Seborg. An Improved PID Switching Control Strategy for Type 1 Diabetes. *IEEE Transactions on Biomedical Engineering*, 55(3):857–865, mar 2008. ISSN 0018-9294. doi: 10.1109/TBME.2008.915665.
11. Rakesh P. Borase, D. K. Maghade, S. Y. Sondkar, and S. N. Pawar. A review of PID control, tuning methods and applications. *International Journal of Dynamics and Control*, 9(2):818–827, 2020. ISSN 21952698. doi: 10.1007/s40435-020-00665-4.
12. Marie Aare Bentsen, Zaman Mirzadeh, and Michael W. Schwartz. Revisiting How the Brain Senses Glucose—And Why. *Cell Metabolism*, 29(1):11–17, jan 2019. ISSN 15504131. doi: 10.1016/j.cmet.2018.11.001.
13. Denis Burdakov, Simon M. Luckman, and Alexei Verkhratsky. Glucose-sensing neurons of the hypothalamus. *Philosophical Transactions of the Royal Society B: Biological Sciences*, 360(1464):2227–2235, dec 2005. ISSN 0962-8436. doi: 10.1098/rstb.2005.1763.
14. Vanessa H. Routh. Glucose-sensing neurons. *Physiology Behavior*, 76(3):403–413, jul 2002. ISSN 00319384. doi: 10.1016/S0031-9384(02)00761-8.
15. Takeshi Sakurai. The neural circuit of orexin (hypocretin): Maintaining sleep and wakefulness, mar 2007. ISSN 1471003X.
16. Takeshi Sakurai, Akira Amemiya, Makoto Ishii, Ichiyo Matsuzaki, Richard M. Chemelli, Hirokazu Tanaka, S. Clay Williams, James A. Richardson, Gerald P. Kozlowski, Shelagh Wilson, Jonathan R.S. Arch, Robin E. Buckingham, Andrea C. Haynes, Steven A. Carr, Roland S. Annan, Dean E. McNulty, Wu Schyong Liu, Jonathan A. Terrett, Nabil A. Elshourbagy, Derk J. Bergsma, and Masashi Yanagisawa. Orexins and orexin receptors: A family of hypothalamic neuropeptides and G protein-coupled receptors that regulate feeding behavior. *Cell*, 92(4):573–585, feb 1998. ISSN 00928674. doi: 10.1016/S0092-8674(00)80949-6.
17. Akihiro Yamanaka, Carsten T. Beuckmann, Jon T. Willie, Junko Hara, Natsuko Tsujino, Michihiro Mieda, Makoto Tominaga, Ken Ichi Yagami, Fumihiro Sugiyama, Katsutoshi Goto, Masashi Yanagisawa, and Takeshi Sakurai. Hypothalamic orexin neurons regulate arousal according to energy balance in mice. *Neuron*, 38(5):701–713, 2003. ISSN 08966273. doi: 10.1016/S0896-6273(03)00331-3.
18. Claudio L. A. Bassetti, Antoine Adamantidis, Denis Burdakov, Fang Han, Steffen Gay, Ulf Kallweit, Ramin Khatami, Frits Koning, Brigitte R. Kornum, Gert Jan Lammers, Roland S. Liblau, Pierre H. Luppi, Geert Mayer, Thomas Pollmächer, Takeshi Sakurai, Federica Sallusto, Thomas E. Scammell, Mehdi Tafti, and Yves Dauvilliers. Narcolepsy — clinical spectrum, aetiopathophysiology, diagnosis and treatment. *Nature Reviews Neurology*, 15(9):519–539, sep 2019. ISSN 1759-4758. doi: 10.1038/s41582-019-0226-9.
19. Christelle Peyron, Devin K. Tighe, Anthony N. Van Den Pol, Luis De Lecea, H. Craig Heller, J. Gregor Sutcliffe, and Thomas S. Kilduff. Neurons containing hypocretin (orexin) project to multiple neuronal systems. *Journal of Neuroscience*, 18(23):9996–10015, 1998. ISSN 02706474. doi: 10.1523/jneurosci.18-23-09996.1998.
20. Denis Burdakov. Physiological Changes in Glucose Differentially Modulate the Excitability of Hypothalamic Melanin-Concentrating Hormone and Orexin Neurons In Situ. *Journal of Neuroscience*, 25(9):2429–2433, mar 2005. ISSN 0270-6474. doi: 10.1523/JNEUROSCI.4925-04.2005.
21. Antonio J. Gonzalez, Lise T. Jensen, Lars Fugger, and Denis Burdakov. Metabolism-Independent Sugar Sensing in Central Orexin Neurons. *Diabetes*, 57(10):2569–2576, oct 2008. ISSN 0012-1797. doi: 10.2337/db08-0548.
22. Antonio J. González, Panagiota Iordanidou, Molly Strom, Antoine Adamantidis, and Denis Burdakov. Awake dynamics and brain-wide direct inputs of hypothalamic MCH and orexin networks. *Nature Communications*, 7(1):11395, apr 2016. ISSN 2041-1723. doi: 10.1038/ncomms11395.
23. Takeshi Sakurai, Ruby Nagata, Akihiro Yamanaka, Hiroko Kawamura, Natsuko Tsujino, Yo Muraki, Haruaki Kageyama, Satoshi Kunita, Satoru Takahashi, Katsutoshi Goto, Yoshimasa Koyama, Seiji Shioda, and Masashi Yanagisawa. Input of Orexin/Hypocretin Neurons Revealed by a Genetically Encoded Tracer in Mice. *Neuron*, 46(2):297–308, apr 2005. ISSN 08966273. doi: 10.1016/j.neuron.2005.03.010.
24. William J. Giardino, Ada Eban-Rothschild, Daniel J. Christoffel, Shi-Bin Li, Robert C. Malenka, and Luis de Lecea. Parallel circuits from the bed nuclei of stria terminalis to the lateral hypothalamus drive opposing emotional states. *Nature Neuroscience*, 21(8):1084–1095, aug 2018. ISSN 1097-6256. doi: 10.1038/s41593-018-0198-x.
25. Go Yoshimichi, Hironobu Yoshimatsu, Takayuki Masaki, and Toshiie Sakata. Orexin-A Regulates Body Temperature in Coordination with Arousal Status. *Experimental Biology and Medicine*, 226(5):468–476, jan 2001. ISSN 1535-3702. doi: 10.1177/153537020122600513.
26. Rhîannan H Williams and Denis Burdakov. Hypothalamic orexins/hypocretins as regulators of breathing. *Expert Reviews in Molecular Medicine*, 10(0):e28, oct 2008. ISSN 1462-3994. doi: 10.1017/S1462399408000823.
27. Mahesh M. Karnani, Cornelia Schöne, Edward F. Bracey, J. Antonio González, Paulius Viskaitis, Han Tao Li, Antoine Adamantidis, and Denis Burdakov. Role of spontaneous and sensory orexin network dynamics in rapid locomotion initiation. *Progress in Neurobiology*, 187:101771, apr 2020. ISSN 18735118. doi: 10.1016/j.pneurobio.2020.101771.
28. Ben Engelhard, Joel Finkelstein, Julia Cox, Weston Fleming, Hee Jae Jang, Sharon Ornelas, Sue Ann Koay, Stephan Y. Thiberge, Nathaniel D. Daw, David W. Tank, and Ilana B. Witten. Specialized coding of sensory, motor and cognitive variables in VTA dopamine neurons. *Nature*, 570(7762):509–513, 2019. ISSN 14764687. doi: 10.1038/s41586-019-1261-9.
29. B. K. Anand, G. S. Chhina, K. N. Sharma, S. Dua, and Baldev Singh. Activity of single neurons in the hypothalamic feeding centers: effect of glucose. *American Journal of Physiology-Legacy Content*, 207(5):1146–1154, nov 1964. ISSN 0002-9513. doi: 10.1152/ajplegacy.1964.207.5.1146.
30. Y. Oomura, T. Ono, H. Ooyama, and M. J. Wayner. Glucose and Osmosensitive Neurones of the Rat Hypothalamus. *Nature*, 222(5190):282–284, apr 1969. ISSN 0028-0836. doi: 10.1038/222282a0.
31. Roger Carpenter and Benjamin Reddi. *Neurophysiology: A Conceptual Approach*. 2012. ISBN 978-1444135176.
32. Junko Hara, Carsten T. Beuckmann, Tadahiro Nambu, Jon T. Willie, Richard M. Chemelli, Christopher M. Sinton, Fumihiro Sugiyama, Ken-ichi Yagami, Katsutoshi Goto, Masashi Yanagisawa, and Takeshi Sakurai. Genetic Ablation of Orexin Neurons in Mice Results in Narcolepsy, Hypophagia, and Obesity. *Neuron*, 30(2):345–354, may 2001. ISSN 08966273. doi: 10.1016/S0896-6273(01)00293-8.
33. Mahesh K. Karnani and Denis Burdakov. Multiple hypothalamic circuits sense and regulate glucose levels. *American Journal of Physiology-Regulatory, Integrative and Comparative Physiology*, 300(1):R47–R55, jan 2011. ISSN 0363-6119. doi: 10.1152/ajpregu.00527.2010.
34. Chun-Xia Yi, Mireille J. Serlie, Mariette T. Ackermans, Ewout Foppen, Ruud M. Buijs, Hans P. Sauerwein, Eric Fliers, and Andries Kalsbeek. A Major Role for Perifornical Orexin Neurons in the Control of Glucose Metabolism in Rats. *Diabetes*, 58(9):1998–2005, sep 2009. ISSN 0012-1797. doi: 10.2337/db09-0385.
35. Vagner R. Antunes, G. Cristina Brailoiu, Ernest H. Kwok, Phouangmala Scruggs, and Nae J. Dun. Orexins/hypocretins excite rat sympathetic preganglionic neurons in vivo and in vitro. *American Journal of Physiology-Regulatory, Integrative and Comparative Physiology*, 281 (6):R1801–R1807, dec 2001. ISSN 0363-6119. doi: 10.1152/ajpregu.2001.281.6.R1801.
36. Antoine R. Adamantidis, Feng Zhang, Alexander M. Aravanis, Karl Deisseroth, and Luis de Lecea. Neural substrates of awakening probed with optogenetic control of hypocretin neurons. *Nature*, 450(7168):420–424, nov 2007. ISSN 0028-0836. doi: 10.1038/nature06310.
37. Ralph A. DeFronzo, Ele Ferrannini, Leif Groop, Robert R. Henry, William H. Herman, Jens Juul Holst, Frank B. Hu, C. Ronald Kahn, Itamar Raz, Gerald I. Shulman, Donald C. Simonson, Marcia A. Testa, and Ram Weiss. Type 2 diabetes mellitus. *Nature Reviews Disease Primers*, 1(1):15019, dec 2015. ISSN 2056-676X. doi: 10.1038/nrdp.2015.19.
38. Antonio J. González, Lise T. Jensen, Panagiota Iordanidou, Molly Strom, Lars Fugger, and Denis Burdakov. Inhibitory Interplay between Orexin Neurons and Eating. *Current Biology*, 26(18):2486–2491, sep 2016. ISSN 09609822. doi: 10.1016/j.cub.2016.07.013.
39. Paulius Viskaitis, Myrtha Arnold, Celia Garau, Lise T. Jensen, Lars Fugger, Daria Peleg-Raibstein, and Denis Burdakov. Ingested non-essential amino acids recruit brain orexin cells to suppress eating in mice. *Current Biology*, pages 1–10, mar 2022. ISSN 09609822. doi: 10.1016/j.cub.2022.02.067.
40. Joshua Kim, Michele Pignatelli, Sangyu Xu, Shigeyoshi Itohara, and Susumu Tonegawa. Antagonistic negative and positive neurons of the basolateral amygdala. *Nature Neuroscience*, (October):1–15, 2016. ISSN 1097-6256. doi: 10.1038/nn.4414.

Supplementary Figures

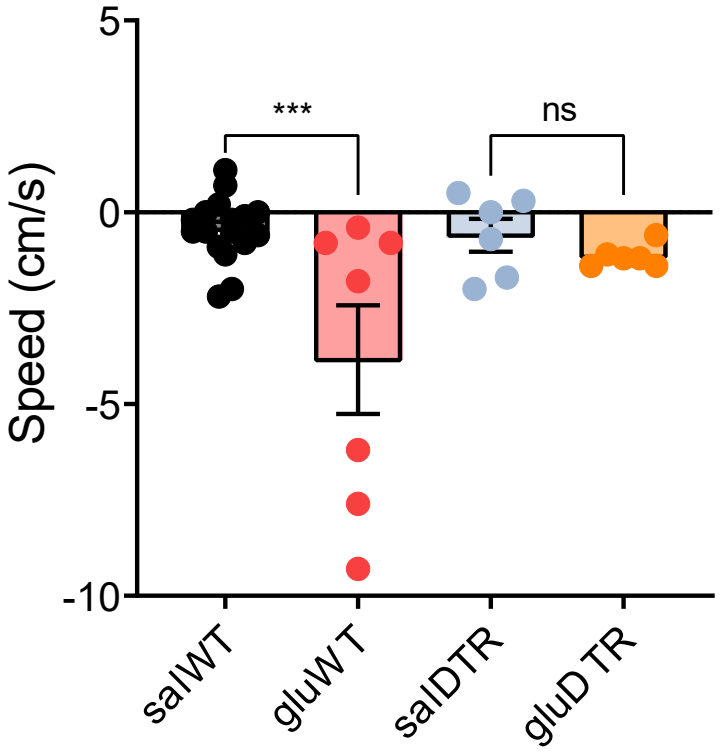

Supplementary Figure 1 - Inhibition of running by glucose is abolished in HON-ablated DTR mice. Related to Figures 1, 4 and 5.

Wildtype mice (WT) demonstrate a significant suppression of running after glucose (glu) infusion compared to saline (sal). This effect was abolished in HON-ablated (DTR) animals. ANOVA F (3, 32) = 6.399; p = 0.0016; Holm-Šídák's multiple comparisons tests: salWT vs. gluWT p = 0.0003, salDTR vs. gluDTR p = 0.5956. Outliers eliminated by ROUT 1% test. Glucose administration and analysed time period correspond to those in Figures 4 and 5. Data are presented as means and SEM.

A

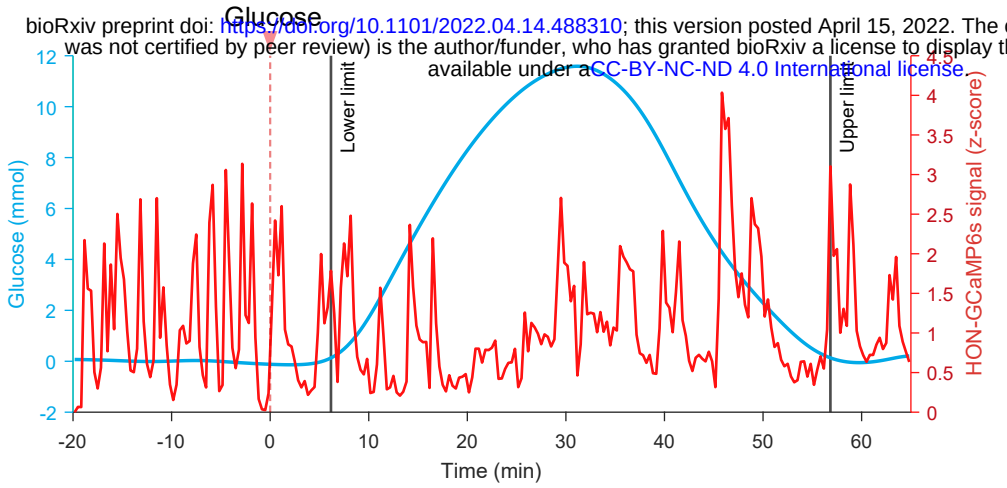

B

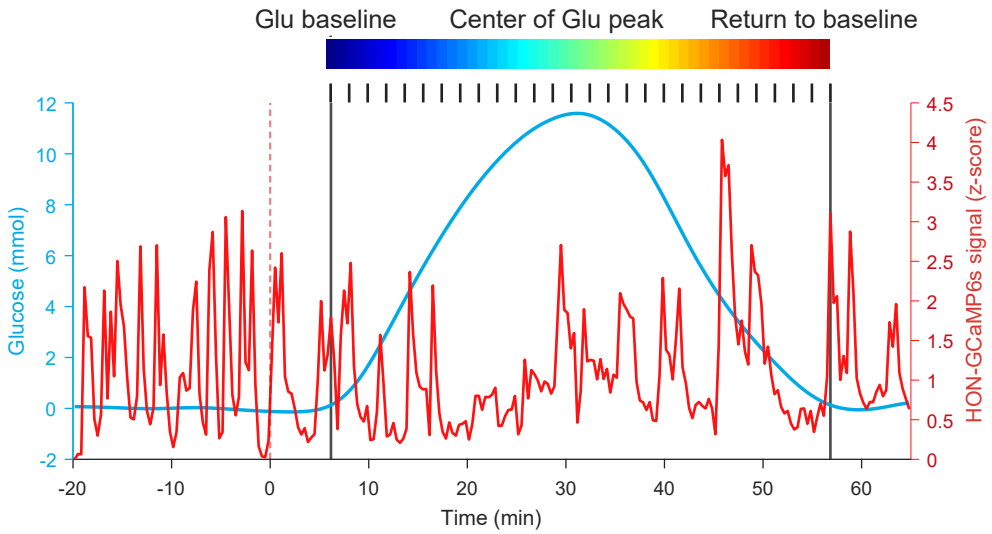

Supplementary Figure 2 - Algorithm for plotting the relationship between blood glucose concentration and HON activity. Related to Figure 2.

(A) Example HON-GCaMP6s activity trace (red) and blood glucose levels (blue). Traces were were temporally aligned and boundaries of blood glucose peak were identified (black; glucose must be <5% of peak level and change < 0.15 mM/min).

(B) Time period between blood glucose peak boundaries was subdivided into 50 equal periods, and average blood glucose and HON activity values were obtained. Temporal relationship was displayed by color-coding these values from blue to green to red.

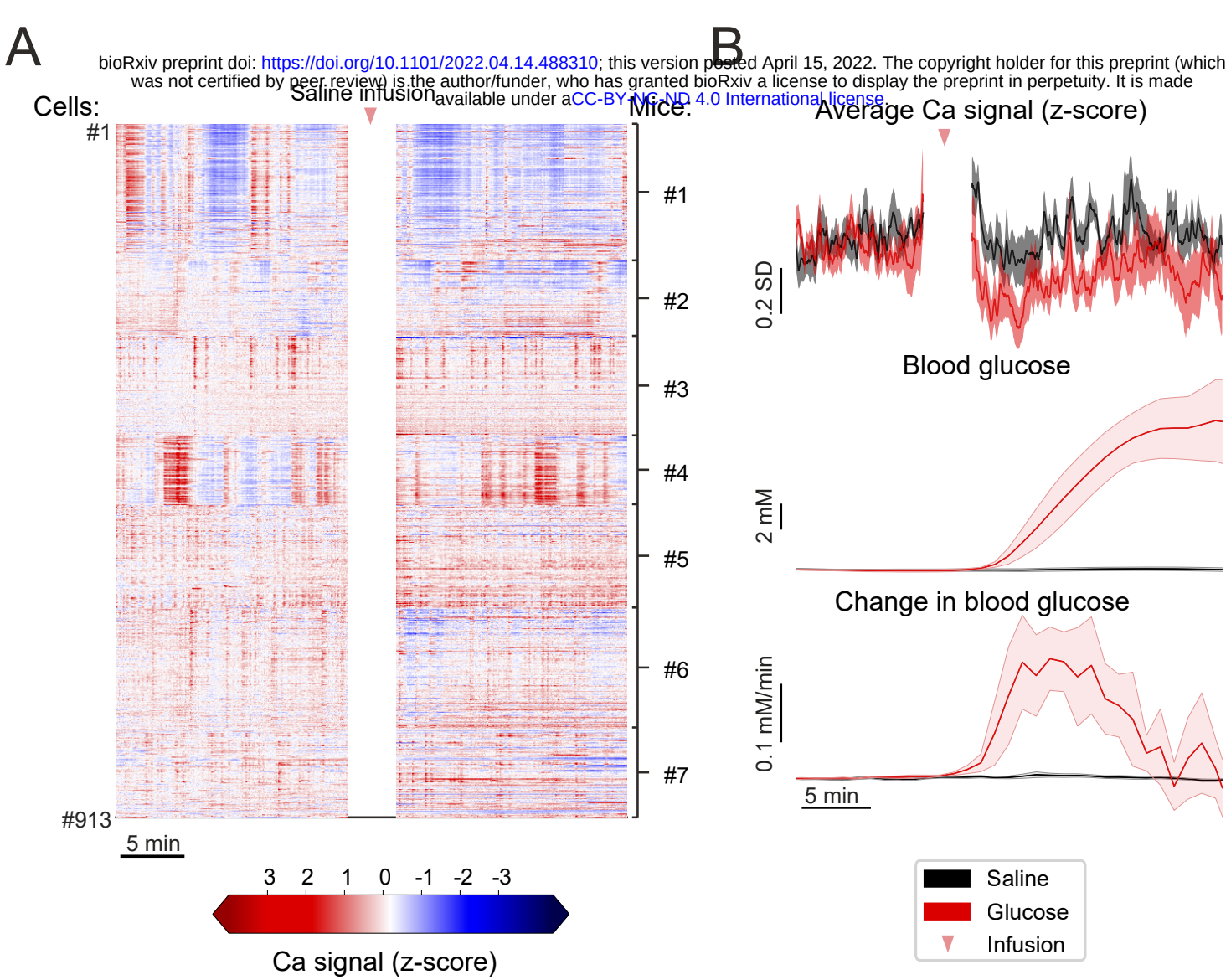

Supplementary Figure 3 - Single cell HON responses to saline and glucose infusions. Related to Figure 4.

(A) Individual responses of 913 HONs to saline infusion from 7 mice.

(B) Temporal alignment of average HON responses (top) to blood glucose concentration (middle) and its derivative (bottom) after saline or glucose infusions.

Breaks in the neural recordings are due to laser shutter being closed during infusions in majority of the experiments. Data are presented as means and SEM.